PROGRESS REVIEW

Large-area molecular monolayer-based electronic junctions with transferred top electrodes

View the article online for updates and enhancements.

PROGRESS REVIEW

Large-area molecular monolayer-based electronic junctions with transferred top electrodes

Wang-Taek Hwang[1], Yeonsik Jang[1], Minwoo Song[1], Dong Xiang[2], and Takhee Lee[1*]

[1]Department of Physics and Astronomy, and Institute of Applied Physics, Seoul National University, Seoul 08826, Republic of Korea
[2]Tianjin Key Laboratory of Optoelectronic Sensor and Sensing Network Technology, College of Electronic Information and Optical Engineering, Nankai University, 300071, People's Republic of China

*E-mail: tlee@snu.ac.kr

Vertical structure of ensemble molecular electronic junction is a widely used platform for investigating the electrical properties of molecular monolayers. Direct metal deposition on the molecular layer, however, causes the shorted circuit problem in the most junctions. One of the methods to avoid this problem is transferring pre-made electrodes on the molecular layer. This article reviews the large-area molecular electronic junctions fabricated in such a way and discusses about their fabrication process, device yield, electrical properties, and applications. The earlier part of this article introduces the molecular junctions with metal (e.g. Au) electrodes transferred in various methods. In the later part, the electrical characteristics and functionalities of the molecular junctions adapting the graphene electrodes are reviewed.
© 2020 The Japan Society of Applied Physics

1. Introduction

Since the theoretical study by Aviram and Ratner in 1974,[1] molecular electronics has drawn a great interest because single-molecules or molecular layers can be utilized as electronic transport channels. The major goal in this research field is understanding of intrinsic properties of the molecules, at the same time the experiment techniques including molecular synthesis, device fabrication, measurement and analysis have also been important topics in molecular electronics. Fabrication of molecular junctions is still a challenging issue because it is difficult to connect the small molecules in length scale of ∼1 nm to two electrical leads for electrical measurements.

Single-molecular junctions are a traditional platform to study the electronic transport in molecular wire. Scanning tunneling microscope[2,3] conducting probe atomic force microscope[4] are widely used tools that build the molecular junctions by contacting their tips to the molecular layer deposited on the specific surfaces. Another way to fabricate the single-molecular junction is to insert the molecule into a nano-gap of broken wire. Electro-migration break junction[5–7] and mechanically controllable break junction[8,9] are representative methods to create nano-gap in the wire.

Another testbed for the experiment in molecular electronics is large-area ensemble molecular junction in which many molecules (> ∼1000 molecules) exist in the junction and are involved in the charge transport. Typical structure of these junctions is a vertical stack of "bottom electrode—molecular layer—top electrode." Molecular monolayer can be deposited on the surface of bottom electrode by using the self-assembly nature of molecules with certain end-groups, so such molecular layer is called self-assembled monolayer (SAM). For example, thiol (-SH) moiety of a molecule makes covalent bonds with Au, Ag, or Pt surfaces.[10] Langmuir–Blodgett (LB) film[11,12] is also used for preparing homogeneous molecular layer by utilizing the surfactant molecules arranging at air-solvent interface.

Forming the top electrode on the molecular layer is the major challenge in building the large-area molecular junctions. The simplest way for that is direct deposition using thermal or electron-beam evaporator, but this method makes most junctions electrically shorted because metal filaments are grown through the thin molecular layer.[13,14] To enhance the junction yield, buffer interlayer-based junction[15–17] or liquid metal contact[18–20] were introduced. Several studies about large-area molecular junctions fabricated by "electrode-transfer"[21–28] have been reported, in which pre-made electrodes on the dummy substrate are transferred on the molecular layer. Since the transferred electrodes make contact with molecular layer without metal filaments, this is an alternative fabrication method for molecular junctions that do not damage the molecular layer and secures high device yield.

In this article, we review the molecular electronic junctions with the transferred top electrodes in terms of materials for the electrodes (e.g. Au and graphene) and summarize their fabrication processes, electrical properties, and application for the functional molecular junctions.

2. Molecular junctions with transferred gold electrode

2.1. Overview

Nanopore or *via*-hole technique[29,30] are traditional method fabricating the large-area ensemble molecular junctions in which the top metal contact is created by direct vacuum evaporation. They are suitable for investigation about the intrinsic transport in molecular wire because pure metal-molecule-metal junctions are ensured but applying them to the practical devices is difficult due to their low device yield (∼1%). Employing conducting polymer as buffer interlayer[15–17] or liquid metal contact of eutectic GaIn[18–20] makes a huge improvement in device yield but ambiguity at molecule-interlayer has been remained. Therefore, gold electrode-transfer is suitable testbed to study the transport across molecule-metal interface while satisfying moderate device yield for practical application. Several kinds of the molecular junctions by gold electrode-transfer have been reported. Their device fabrication processes and schematics are summarized in Fig. 1 and the detailed explanations for each junction are in following sections.

2.2. Nano-transfer printing

Figure 1(a) illustrates the molecular junction fabricated in nano-transfer printing (nTP) technology introduced by
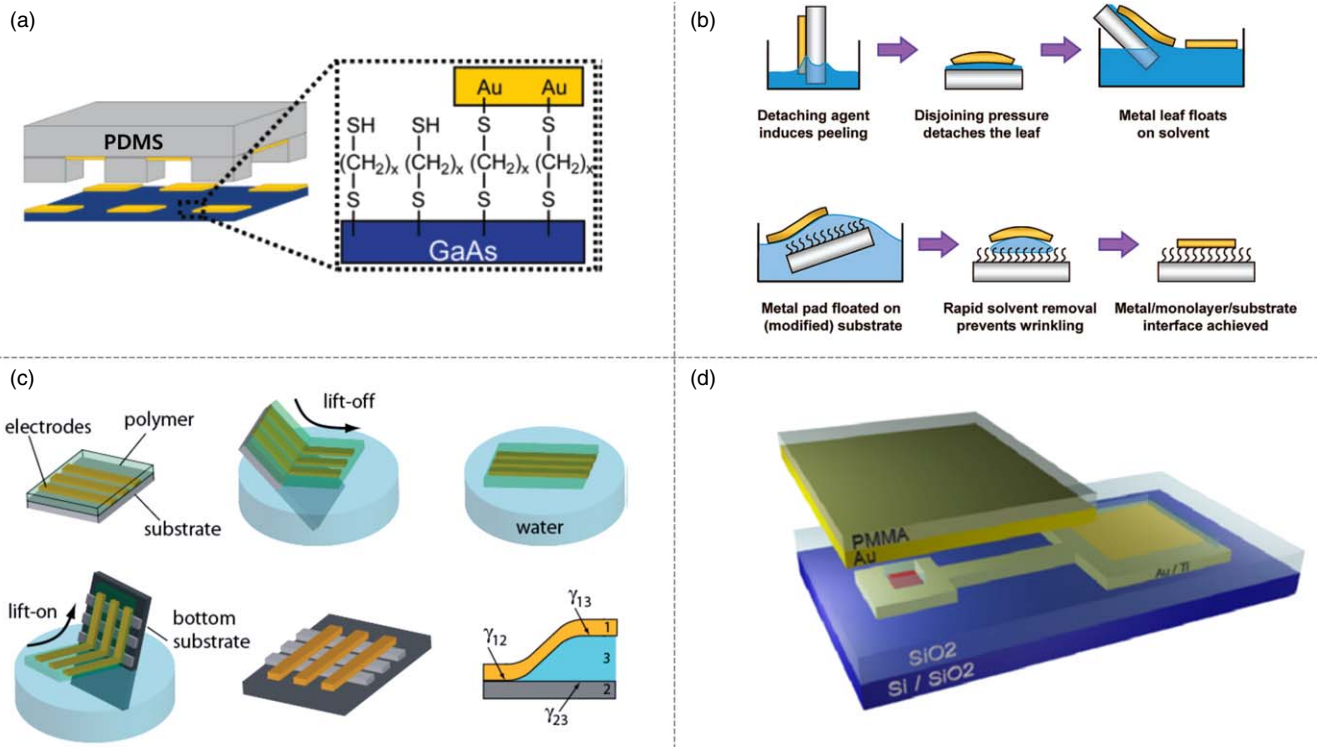
Fig. 1. (Color online) Schematics for fabrication procedure of large-area molecular junctions by (a) nanotransfer printing (nTP) (Reproduced with permission from Ref. 21. Copyright 2003 American Chemical Society), (b) lift-off float-on (LOFO) (Reproduced with permission from Ref. 31. Copyright 2008 American Chemical Society), (c) polymer-assisted lift-off (PALO) (Reproduced with permission from Ref. 23. Copyright 2006 John Wiley & Sons), and (d) direct metal transfer (DMT) (Reproduced with permission from Ref. 24. Copyright 2014 IOP Publishing).

Loo et al.[21] It is obtained by transferring the metal film onto the molecule-treated substrate from the elastomeric poly-(dimethylsiloxane) (PDMS) stamp. In this work, GaAs/SAM/Au junctions are fabricated with various junction area and their electric characteristics are shown in comparisons with junctions fabricated by direct metal evaporation method to provide insight into how top metal film fabrication affects the electrical transport in molecular electronic junctions.

To fabricate nTP molecular junctions, the conductive n^+ GaAs substrate is prepared for the bottom electrode of the junctions. After chemical etching the surface to remove native oxide, the substrate is immediately exposed to saturated molecular vapor of octanedithiol (DC8) in a desiccator. Only one end of molecules reacts with the GaAs surface and monolayer of DC8 is self-assembled on the surface. Then a fresh gold-coated PDMS stamp is brought into contact with the SAM-treated GaAs substrate without applying additional pressure. To release the Au pattern from the stamp, the surface chemistry must be considered. The spontaneous chemical bonding of S–Au at the SAM/Au interface facilitates the pattern transfer. In addition to providing strong adhesion between Au pattern and GaAs substrate, DC8 molecular layer serves as the electrical component in these molecular junctions.

The current–voltage (I–V) measurements for nTP molecular junction with different contact areas (circular Au patterns with diameters of 62.5, 125, 250, and 500 μm) were performed and the results are depicted in Fig. 2(a). The scaling of total current with contact area shows the uniform current distribution in nTP junctions. The specific resistances
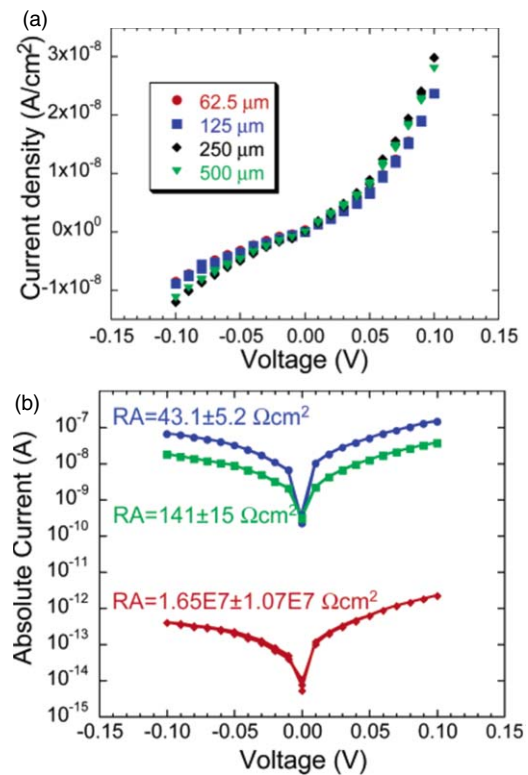
Fig. 2. (Color online) Electrical characteristics of nTP junctions (a) current density as a function of applied voltage. (b) Absolute current levels (on a log scale) for applied voltage; control sample (blue circles). Evaporated sample (green squares). nTP samples (red diamonds). Reproduced with permission from Ref. 21. Copyright 2003 American Chemical Society.

(RA, R is the slope in the small bias region of the I–V curve, A is the contact area) for almost devices are also distributed within an order of magnitude. These results show that nTP is an effective fabrication method for reliable and reproducible molecular electronic devices.

Figure 2(b) shows I–V curves for the control (GaAs/Au junction), evaporated and nTP junctions with the same contact area. The effective barrier heights in each junction can be obtained by analyzing the electrical characteristics with the thermionic emission model. The extracted effective barrier heights of the control and evaporated junctions are 0.55 and 0.58 V which are lower values than the Schottky barrier height at n^+ GaAs/Au interface (0.7 V). These results indicate the generation of the ohmic contact, which are consistent with the large current densities for the control and evaporated junctions. However, the higher effective barrier height ($\sim$0.9 V) extracted from the I–V curve of nTP junction implies that the ohmic fraction is not present, thus tunneling through the molecular layer can be major transport channel in these junctions. The transport through ohmic contact in the evaporation sample and the tunneling through SAM in the nTP sample make the deviation of effective barrier heights from the ideal Schottky contact in opposite direction.

Although this early work for nTP junction introduced the platform of mass production of high-yield molecular devices with various junction area and which enabled the statistical analysis, one challenge was the rough surface of top electrode generated during metal evaporation on the PDMS stamp. Roughness of electrode may generate small vacancies at SAM/metal electrode, which lead unreliable electrical properties.

2.3. Lift-off and float-on approach

Thin metal films floating on the surface of liquid would be applied as the top electrode of molecular junctions. Figure 1(b) illustrates the device fabrication procedure based on such idea, termed as "lift-off, float on (LOFO)", developed by Cahen et al.[31] Metal film deposited on the clean glass slide detached by etching solution then the "metal leaf" leaves to float on the solvent with proper surface tension [upper part in Fig. 1(b)]. Molecular treated substrate is lifted with the leaf on top and the vertical structure of metal/molecule/substrate is made with the help of capillary interaction during drying the common liquid [lower part in Fig. 1(b)]. Comprehensive study for generating the LOFO junctions was also reported,[32] which accounts for the major forces related to the process. This work introduces the major challenges and provides solutions in qualitative manner.

Several kinds of molecular junctions with different semiconductor substrates such as GaAs,[22] Si,[33] and ZnO[34] were investigated. In these studies, the effects of molecular dipole at metal/semiconductor interface for electrical characteristics were discussed. Figure 3 shows the different I–V curves in the GaAs/molecule/Au junctions fabricated in LOFO method.[22] By using the nature dicarboxylic acid group that bonding to GaAs, molecular monolayers of tartaric acid derivatives (inset of Fig. 3) are deposited on GaAs substrate. Systematic modification of the molecular dipole is possible by the substituted benzene groups with various substituents in this work. Compared to the control junction (bare), molecularly modified GaAs/Au diodes show the change in
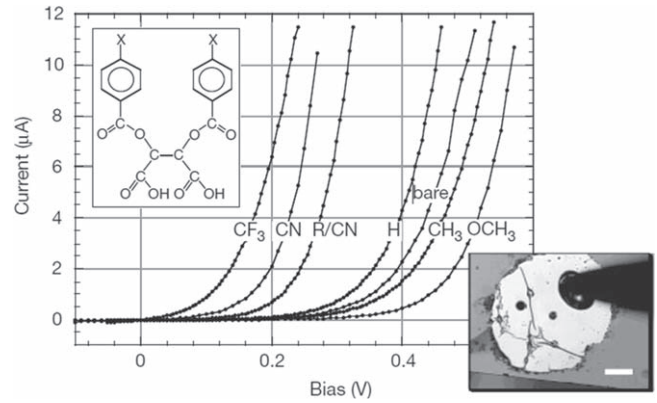
Fig. 3. Electrical characteristics of LOFO junctions. Main figure is the different I–V curves refer to the junctions of different substituent on the benzene ring (shown next to each curve) of the dicarboxylic acid derivatives (see inset). Bottom right inset is optical micrograph (scale bar, 100 μm) of Au pad. Reproduced with permission from Ref. 22. Copyright 2000 Springer Nature.

I–V characteristics depending on the direction and magnitude of each molecular dipoles. It is shown that the effective barrier height in diode junction is modified by the dipole moment of the substituted benzene, which results in changes in I–V characteristics. These barrier heights are also related to the work function of the surface but only limited fraction in the changed of work function is expressed in the effective barrier heights in the junctions based on GaAs substrate because the Schottky–Mott rule that used to extract the barrier height in this work is not suitable tool for the covalent semiconductor like GaAs with high density of surface states. Later study, in which GaAs is replaced by ZnO (ionic semiconductor), shows the effective modulation in barrier heights depending on the work function of the surfaces treated by different molecules.[34]

2.4. Electrode-transfer based on the polymer film

Another way to build top electrode on the molecular layer is to transfer the metal film with assistance of thin polymer film. The differentiations of this method from the imprinting technique are as follows; (i) ultraflat surface of top electrode originates from the dummy substrate, (ii) surface chemistry to release the metal film from the stamp is less important since the polymer film is washed out when the junction is complete.

Figure 1(c) illustrates the fabrication procedure for one of these methods, termed as polymer-assisted lift-off (PALO).[23] Gold electrode is patterned on ultrasmooth, sacrificial substrate (Si or mica). Poly(methyl methacrylate) (PMMA) or poly(styrene) is then coated covering the whole surface. The electrodes with a PMMA film are detached from the dummy substrate by immersing the sample into the basic solution which weakens the adhesion between the polymer film and substrate. This film is then transferred onto the molecule-treated bottom electrode. After drying the common liquid (water), PMMA is removed by organic solvent. The wrinkle-free electrode is explained by the surface energies (γ) at each interface. Hydrophobicity of gold-PMMA film and molecular monolayer means the high surface energy (γ_{13} and γ_{23}) at the interface with water, which drives water out and makes fine contact between top electrode and molecular layer. In this work, Fatty acids, $CH_3(CH_2)_{n-2}COOH$ with

various molecular lengths are deposited on the bottom electrode by LB film method. The conductivity (σ) in the low bias regime can be expressed by a model for non-resonant tunneling, in which the conductivity is decayed exponentially as the width of tunneling barrier increases. This relationship can be approximately expressed by Simmons equations, where σ_0 is a constant that depends on the system and includes contact resistance, d (Å) is the width of the tunneling barrier, and β (Å^{-1}) is the decay coefficient.

$$\sigma = \sigma_0 e^{-\beta d}. \tag{1}$$

Figure 4(a) is the semi-log plot of the conductivity versus the molecular lengths of fatty acids, which is consistent with the Simmons model. Molecular switching devices with a bistable [2] rotaxane molecules is also demonstrated in the platform of PALO in which the conductivity is switched by the redox process inside the molecule.[35] Small bias is applied across the junctions to read "remnant" current after write voltage pulse. Their switching property is shown in Fig. 4(b), in which the current rapidly switches the states with the threshold voltages of 1 V for turning on and -0.6 V for turning off.

Figure 1(d) shows another example of polymer-assisted electrode-transfer, termed as "direct metal transfer (DMT)".[24] This method is similar to PALO junction but the gold electrode-transfer onto "*via*-hole" structure of which bottom gold electrode is exposed through the hole by etching the insulating layer. Alkanethiolates (denoted as C8, C12, and C16) are used in this work, and their electrical properties are investigated statistically [Figs. 5(a) and 5(b)]. The decay
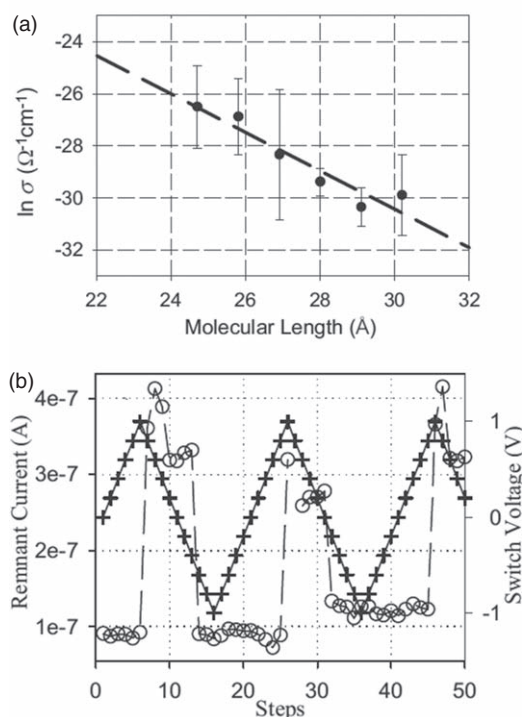
Fig. 4. Electrical characteristics of PALO junctions. (a) Semi-log plot of the tunneling conductivity versus chain-length of fatty acid monolayers. The fit to a straight line gives a slope of $\beta = 0.86$ Å^{-1}. (b) Temporal plot of the remnant current (circles) as a function of applied bias (crosses), displaying switching behavior upon reaching a threshold voltage: 1 V for turning "on" and –0.6 V for turning "off". Reproduced with permission from Ref. 23. Copyright 2006 John Wiley & Sons.

coefficient β ($\sim$1.07 Å^{-1}) and the current independent on the temperature [Figs. 5(c) and 5(d)] imply that the dominant transport mechanism in these junctions is the non-resonant tunneling which follows the Simmons model. The inelastic electron tunneling spectroscopy (IETS) in DMT junction was also measured.[36] IETS is one of the powerful tool for the detection of unique vibration modes of molecules in a tunneling junction. This spectroscopy captures the specific vibration mode of the molecule when electrons tunnel inelastically by delivering an energy quantum into a localized vibrational mode of the molecule. At the specific voltage there appears IETS peak in the second derivative of current versus voltage (d^2I/dV^2-V) graph. Figure 5(e) shows the positions of vibration modes in several DMT junctions of C12 molecule, which are consistent with the other studies for IETS measurement of molecular junctions with alkanethiolates.[5,6,37–39]

## 3. Reliable molecular electronic junctions with a multilayer graphene (MLG) electrode

3.1. Overview

Graphene is an ultra-thin two-dimensional sheet of covalently bonded carbon atoms with outstanding electronic properties, chemical stability and mechanical material properties. It is considered to be a good electrode candidate for molecular junctions. Furthermore, large-area, conductive and flexible graphene films have been successfully synthesized by chemical vapor deposition method, with the ability to patterning or creation of a desired size and shape of the film. As mentioned in the previous section, the limitations of the vertical type molecular junctions are their low device yield and hardness to define molecule-electrode interfaces' nature. The low yield of the molecular junction is attributed to metal penetration within top electrode deposition. As an alternative approach to prevent metal penetration, inserting graphene electrode as an interlayer top electrode as a protective layer before top metal evaporation. In particular, molecular electronic junctions using MLG film as a transferred top electrode have demonstrated a reliable device yield and stability over time.[25,26] In this chapter, we summarize the approach for fabricating solid-state molecular monolayer junctions with MLG electrodes and its charge transport characteristics.
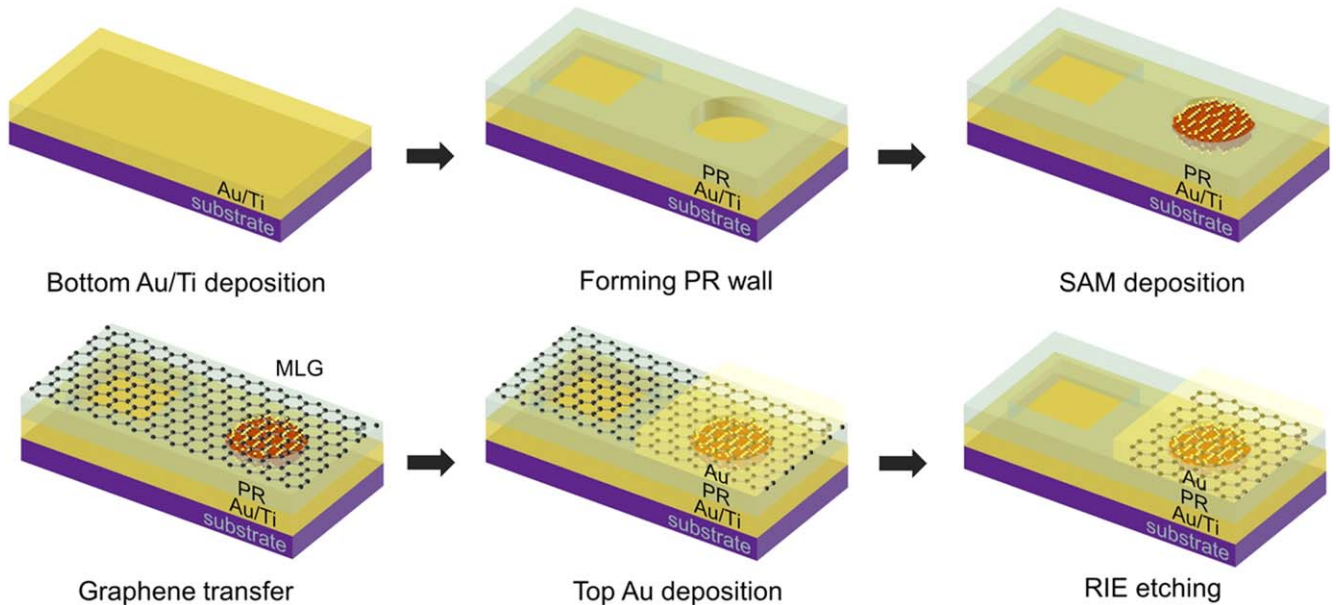
The fabrication process of MLG electrode molecular junctions is followed by the same process for other via-hole structure solid-state vertical junctions. Figure 6 shows the device fabrication procedure. Given bottom electrode patterns on a substrate, via-holes were created by optical lithography. The MLG film transferred onto the hole where SAM deposited on the bottom electrode. The MLG film can be obtained by using MLG grown on Ni or by repeated transfer of single-layer graphene grown on Cu. Deposition of the top metal pad is followed. If single-layer graphenes were used as the interlayer instead of MLG, the evaporated metal atoms might penetrate in this step due to the cracks or pores generated in their growth and transfer processes, which results in the low yield of the molecular junctions.

3.2. Electrical characterization

The typical way to verify that molecular junction with given structure is reliable is to statistically investigate electrical characteristics of device with test-bed molecules such as alkanethiolates or benzenethiolates. Figure 7(a) shows statistical current density–voltage (J–V characteristics for the
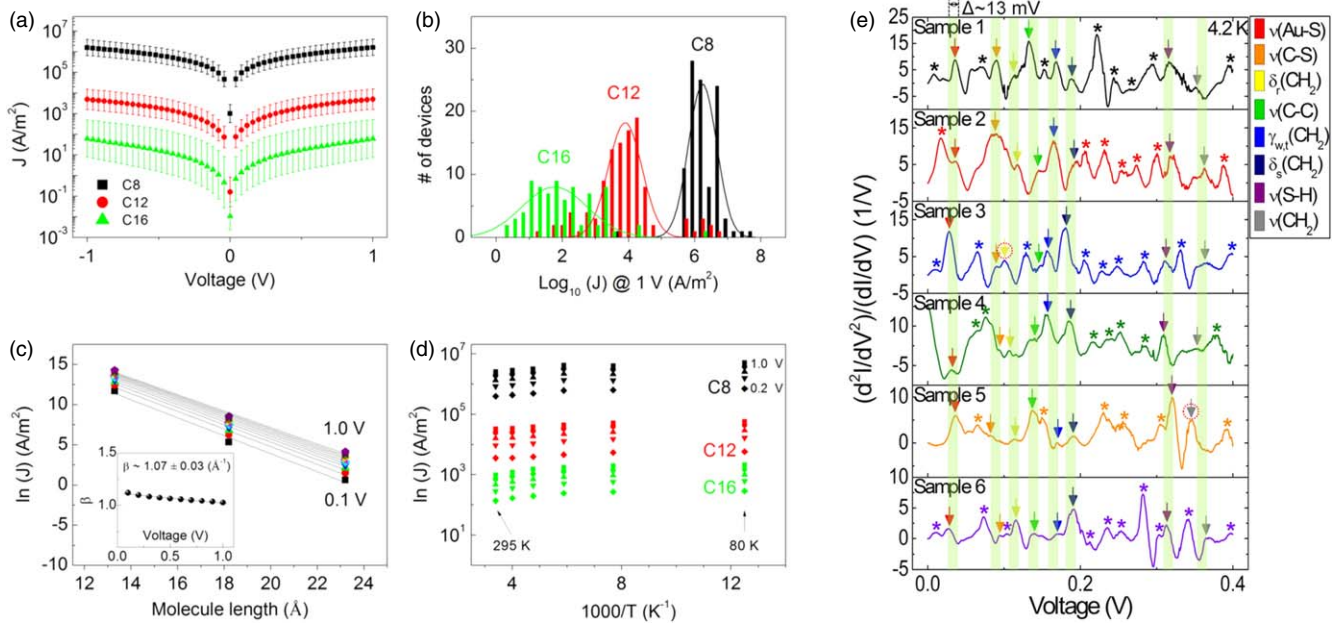
Fig. 5. (Color online) Electrical characteristics of DMT junctions. (a) Statistical J–V data for C8, C12, and C16 working devices. (b) Distribution of the logarithmic current densities at 1 V for all molecular junctions. (c) A semi-log plot of the current densities measured at different biases as a function of the molecular length. Solid lines represent the exponential fitting results, in which the slope is related to the decay coefficient β. The inset shows the values of β deduced from the plot versus the applied bias. (d) Arrhenius plot of the logarithmic current densities for C8, C12 and C16 molecular junctions at different biases from 0.2 to 1.0 V in 0.2 V increments. The temperature was varied from 80 to 295 K in 40 K increments. Reproduced with permission from Ref. 24. Copyright 2014 IOP Publishing. (e) IETS data of six C12 molecular junctions measured at 4.2 K. Each arrow indicates the corresponding molecular vibration modes of the C12 molecule. Peaks that cannot be assigned to any possible vibrational modes of the molecule are marked with asterisks. In this plot, shaded squares are used to compare each characteristic peak from device to device. Reproduced with permission from Ref. 36. Copyright 2015 AIP Publishing.

Fig. 6. (Color online) Schematic illustration of the device fabrication process for the graphene electrode molecular junctions. Reproduced with permission from Ref. 26. Copyright 2016 IOP Publishing.

alkanemonothiol (C8, C12, and C16) and alkanedithiol (DC8) molecular junctions and Fig. 7(b) shows the same for benzenedithol (BDT, BPDT, TPDT) molecular junctions with MLG electrodes. Charge transport mechanism across SAMs of alkanethiolates or benzenethiolates follows the Simmons model mentioned above. As depicted in Fig. 7(c), the decay coefficient β can be easily calculated in the log(J)–V curve, where its absolute value of slope is the same as β. The obtained β value for alkanethiols was about 0.85 Å^{-1}, while 0.33 Å^{-1} for benzeneditholates. These

match well with reference β values.[5,40–47] With temperature-varying current density–voltage (J–V–T) measurement, alkanethiolate and benzenethiolate molecular junctions exhibit temperature-independent J–V, which imply that the primary mechanism of charge transport is non-resonant tunneling.[5,26,47] The durability and operational stability of device are crucial for the practical application. Molecular junctions with graphene electrode show excellent reliability that have long device lifetime without deterioration (more than 40 d), retention characteristics (over 10^4 s).[25] The
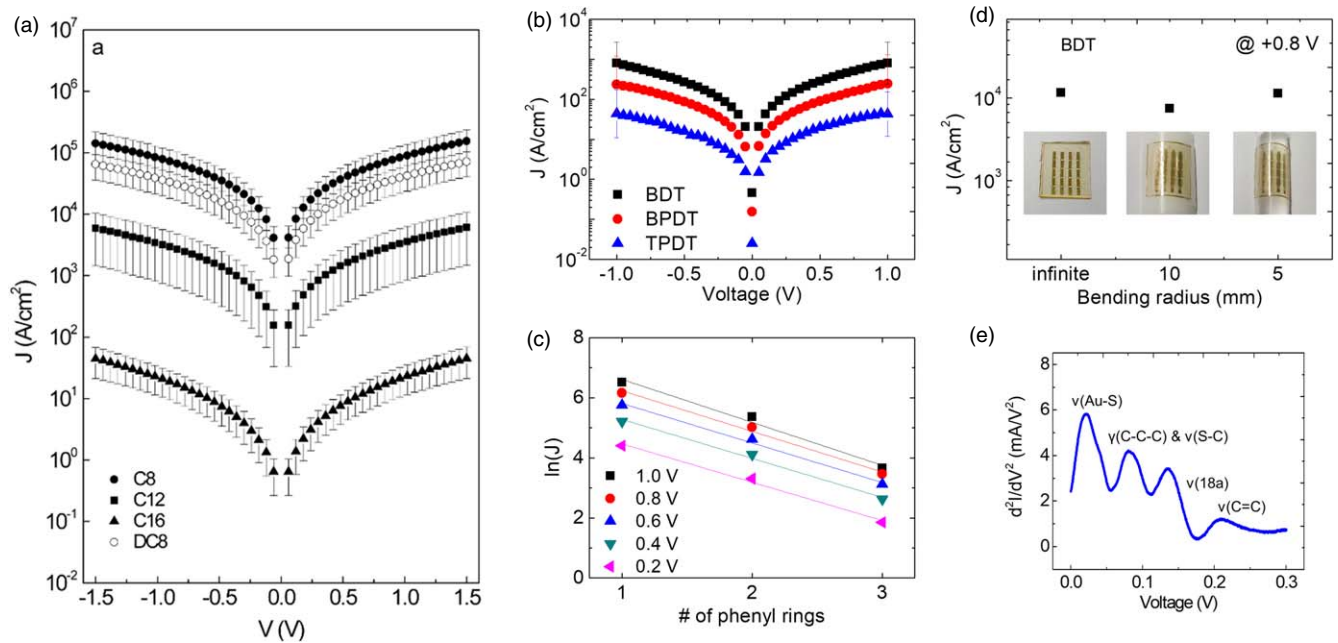
Fig. 7. (Color online) Statistical *J–V* data for all (a) C8, C12, C16 and DC8 molecular junctions (Reproduced with permission from Ref. 25. Copyright 2010 John Wiley & Sons), (b) BDT, BPDT, TPDT molecular junctions. (c) A semi-log plot of the *J* values at different biases versus the numbers of phenyl rings in the BDT, BPDT, and TPDT molecular junctions. (d) Current densities measured at 0.8 V in different bending configurations (bending radii of ∞, 10 mm, and 5 mm). (e) d^2I/dV^2 plot of a BDT molecular junction with a graphene electrode. In the d^2I/dV^2 plot, IETS peaks can be observed at 21, 82, 136, and 209 mV. Reproduced with permission from Ref. 26. Copyright 2016 IOP Publishing.

reliability of the same molecular junctions fabricated on flexible substrate was also demonstrated, under various bending conditions [Fig. 7(d)].[26]

In addition to fundamental current–voltage characterization and temperature-varying measurements, IETS for BDT molecular junctions with graphene electrode was also successfully observed as shown in Fig. 7(e). The IETS peaks are observed at 21, 82, 136, and 209 mV, all of which match with the intrinsic vibration modes of BDT.[6,39,48–50]

3.3. Interface-engineered molecular electronic junctions with chemically doped graphene electrode

As mentioned above, it has been demonstrated that graphene is suitable electrode material for fabrication of reliable molecular junctions. Moreover, it is a promising candidate for interface engineering since its electronic structure can be easily modified by chemical treatment or other external stimuli. A representative demonstration of interface engineering of graphene electrode molecular junction was reported,[28] adopting chemical p-type doping method of a graphene film using trifluoromethanesulfonic acid (CF_3SO_3H, denoted as TFMS). It has been shown that solution-processed p-doping of graphene using TFMS provide high optical transmittance, low sheet resistance, high work function (0.83 eV increase), smooth surface, and air-stability.[51] Figure 8(a) shows the schematic illustration of TFMS-doped graphene.

The molecular junctions were fabricated with benzene-1,4-dithiol (BDT) SAM with pristine (work function of ∼4.4 eV) and TFMS-treated p-doped (work function of ∼5.23 eV) graphene. From statistical analysis, noticeably enhanced charge transport properties and lowered transport barriers for the TFMS-treated p-doped graphene electrode BDT molecular junctions were observed. These phenomena originate from increased hole concentration and decreased hole

injection barrier at the graphene-BDT interface because the main charge transport mechanism of the junction is highest occupied molecular orbital (HOMO)-mediated non-resonant tunneling. In that study, a sufficient number of molecular junctions were fabricated with pristine MLG/BDT/Au (denoted as graphene/BDT/Au) and TFMS-doped MLG/BDT/Au (denoted as TFMS-graphene/BDT/Au) structures. The molecular junctions consisting of the TFMS-doped graphene electrode have been successfully fabricated with a reliable yield (> 70%), Figs. 8(b) and 8(c) show 2-dimensional current density–voltage (*J–V*) plots of all working molecular junctions for the graphene/BDT/Au junctions and TFMS-graphene/BDT/Au junctions. The average current density was increased about one order of magnitude for the TFMS-doped graphene electrode molecular junctions compared to that of the pristine graphene electrode molecular junctions. Transition voltage spectroscopy (TVS) reveals the effective barrier [i.e. the offset between the Fermi energy of the electrode (E_F) and energy level of the HOMO (E_{HOMO})] for electron to tunnel the molecule-electrode interface. The threshold voltage V_T can be obtained from the inflection point of the Fowler-Nordheim plot, which equals the barrier height when applying the Simmons tunneling model.[52,53] As a result of TVS for the graphene/BDT/Au molecular junctions, the average value of V_T was found to be ∼1.08 V and was symmetric for positive and negative voltage polarities. On the other hand, the averaged value of V_T for TFMS-graphene/BDT/Au junctions was found to be ∼0.78 V for both voltage polarities, which was ∼0.3 V lower than that of the graphene/BDT/Au junctions. These results imply that the work function increase of the p-doped graphene electrode lowered the charge injection barrier in the HOMO-dominating molecular tunnel junctions.

(a)

(b)

(c)
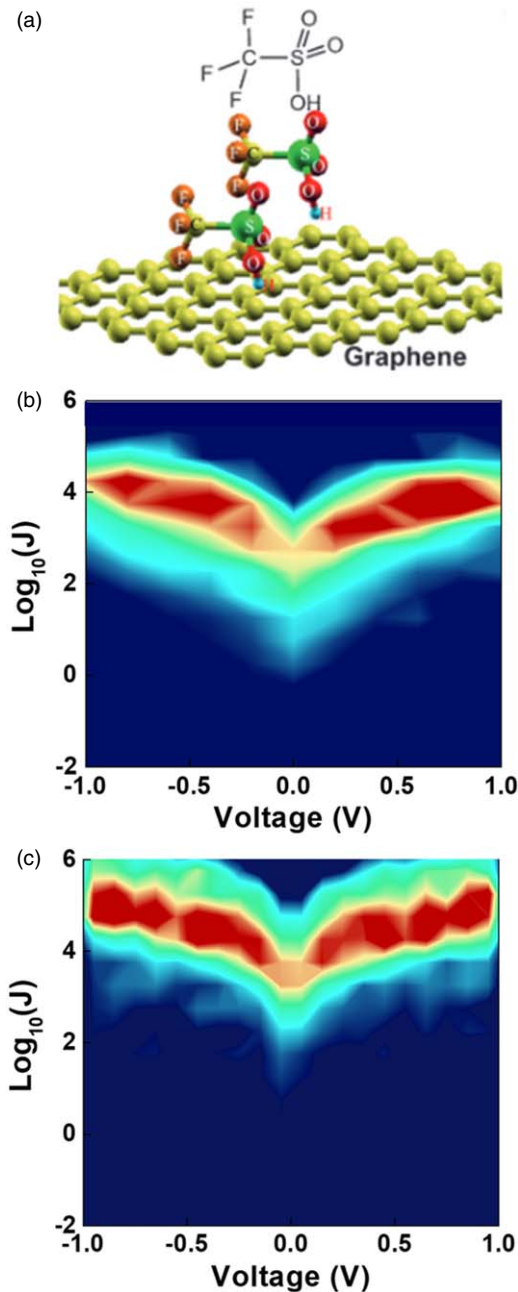
Fig. 8. (Color online) (a) Chemical structure of trifluoromethanesulfonic acid (TFMS) (top) and schematic illustration of TFMS-doped graphene (bottom). Reproduced with permission from Ref. 51. Copyright 2016 John Wiley & Sons. Two-dimensional *J–V* plots of the working molecular junctions for the (b) graphene/BDT/Au and (c) TFMS-graphene/BDT/Au junctions. Reproduced with permission from Ref. 28. Copyright 2017 American Chemical Society.

3.4. Photoswitching molecular junctions with graphene electrodes

To achieve the practical application of molecular electronic devices, a wide range of studies in functional molecular electronics has been carried out over the last decades. One of the most important developments for utilization of functional molecules is photoswitching molecular junctions. Light is useful source for switching devices because of its addressability and compatibility with solid-state device structures. Therefore, the design of photochromic molecules is important for molecular switching devices. In particular, diarylethene (DAE) has been utilized in various ways with the aim to demonstrate bidirectional switching in molecular junctions.

DAEs form a class of photochromes with two different conductance states, i.e. a high conductance (closed; ON) and a low conductance (open; OFF) state. In solution, DAEs can be converted between these two states by illumination with UV or visible light, respectively. This property makes them good candidates for photoswitching molecular junctions due to a large conductance difference between the two states and their response to light.[16,27,54–58] However, the switching behavior of DAE molecular junctions bridged by metal electrodes has been elusive. For example, an Au-DAE-Au junction was only exhibited a unidirectional switching from the closed to the open state.[56] This result is attributed to the quenching of the excited state of the DAE due to strong electronic coupling between the Au metal and the sulfur-based end group, thereby hindering the molecule to adopt its high conductance state.[57] On the other hand, unidirectional switching from the low- to the high conductance state in Au-DAE-Au single-molecule junctions was obtained by modifying the side-arms and end-groups such that they form rigid conjugated molecular wires.[59] These molecules feature a very high quantum yield for the ON switching reaction, but a relatively low one for the OFF switching, explaining the inversed unidirectional switching. In addition, a similar single DAE molecule, bridged between carbon nanotubes[55] or graphene sheets[60] showed a unidirectional switching from the open to the closed state, because strong molecule-electrode couplings between closed state DAE and graphene electrodes enabled the energy transfer from the photoexcited molecule to the extended π-electron system in the electrodes.[61,62]

In recent study, charge transport characteristics of DAE photoswitching molecular junction with MLG electrode were reported.[27] The authors have found that the device can only be switched from the OFF to the ON state, i.e. from the open to the closed state of the employed 1,2-bis(2-methyl-5-(4-mercaptophenylethynyl)furan-3-yl)perfluorcyclopent-1-ene (DAE). Figure 9(a) shows the phototransition properties of the DAE molecular junctions with MLG electrode by real-time current density (*J–t*) measurements. Each data means the open state in the dark (black line), open state exposed to 15 mW UV light (purple line), and closed state exposed to visible light (green line) with the same intensity as the UV light. The current level of the junction in the open state in the dark showed no changes, which suggests that the bias voltage applied to the molecular junction cannot induce the switching. In addition, for the case of the molecular junction prepared in the closed state, the switching behavior could not be observed when exposed to visible light. The only switching behavior that could observe was unidirectional switching from open to closed state. The average switching time was around 680 s, as shown in Fig. 9(b). Note that switching behavior of the DAE molecule is not precisely defined but stochastic and its shape is quite variate among samples.

Figures 9(c) and 9(d) show the fitting curve of experimental I_{exp}–V data with Landauer formalism. The approximate current I_{single} through an equivalent single-molecule junction could be given as

$$I_{single} = \frac{c}{NA}I_{exp} = \frac{2e}{h}\int_{-\infty}^{\infty} T(E)[f_1(E) - f_2(E)]dE. \quad (2)$$

Here, $f_X(E) = (1 + \exp((E - \mu_X)/k_B T))^{-1}$ is the Fermi-Dirac distribution function, where μ_X is the chemical
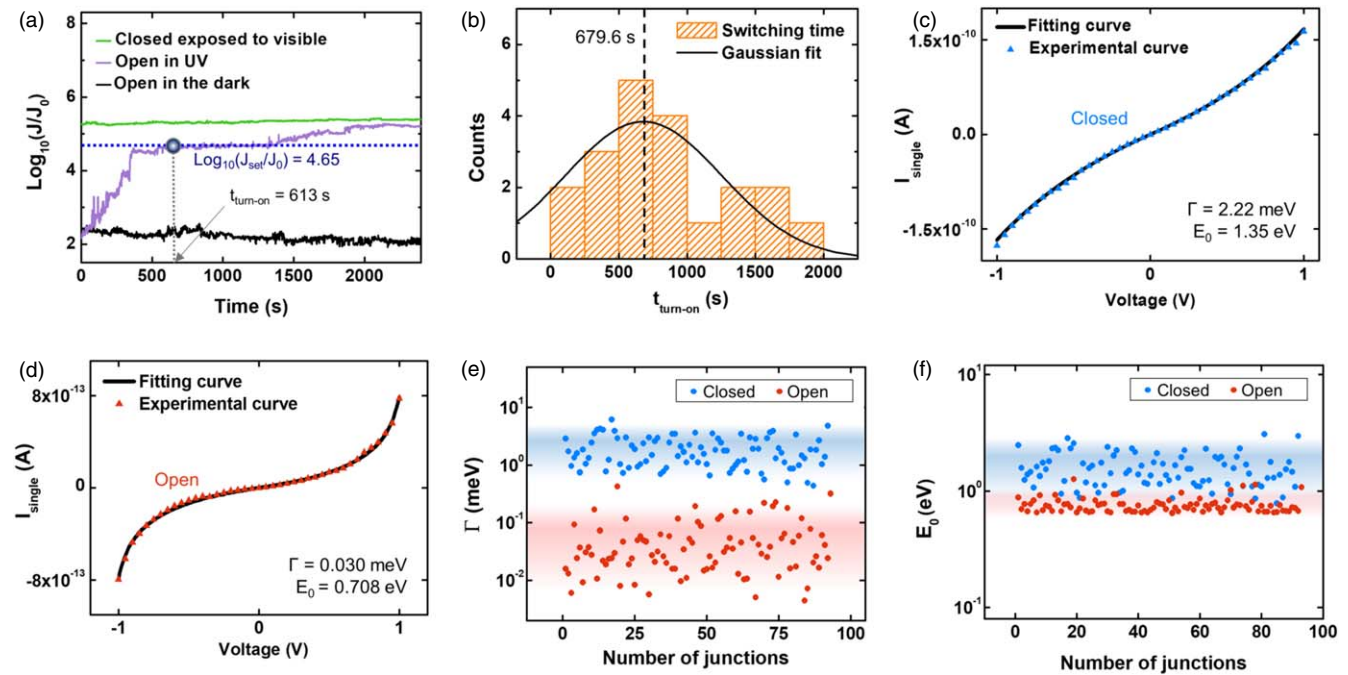
Fig. 9. (Color online) (a) Real-time measurement of the current density for each state with or without exposure to light at an applied bias voltage of 1 V. The switching time (turn-on) is indicted by an arrow. (b) Histogram for the measured switching time required to transition from the open to the closed state. A representative single *I–V* curve measured for the (c) closed and (d) open state, with the fitting curve (shown as a solid line) calculated based on the Landauer formula. Scatter point plots for (e) Γ and (f) E_0 values for intact molecular junctions in the closed and open state. Reproduced with permission from Ref. 27. Copyright 2019 American Chemical Society.

potential of the electrode X = top or bottom. Another factors, N is molecular coverage, c is phenomenological factor that offsets discrepancy between single-molecular junction and SAM junction. The $T(E)$ is a transmission function that was given by single-level symmetric Lorentzian function as below

$$T(E) = \frac{\Gamma^2}{[\Gamma^2 + (E - E_0)^2]}. \tag{3}$$

The E_0 is the difference between the eigen energy of frontier orbital and the Fermi energy of electrode. And Γ indicates the electronic coupling strength of the molecular orbital to the respective electrode. By performing numerical curve fitting, one can calculate the factor E_0 and Γ from each *I–V* curve. Figure 9(c) shows curve fitting result of closed state molecular junction, whereas Fig. 9(d) shows result for open state molecular junction. For all working junctions, the distributions of Γ and E_0 values are presented in the scatter plot in Figs. 9(e) and 9(f). By averaging these distributions, the effective coupling strength Γ for closed and open states was determined to be 1.93 meV and 0.0572 meV, respectively, and the corresponding charge injection barrier E_0 for closed and open states was extracted to be 1.560 meV and 0.756 meV, respectively. In particular, it is notable that the effective value of Γ in the closed state is more than 30 times larger than that of the open state. The relatively strong coupling between DAE and MLG electrodes in the closed state may also cause the unidirectional switching. It is possible that the strong interaction between the closed state of the DAE molecules and the electrode can quench the photo-excited closed state, effectively disturbing the switching process and eventually preventing the transition to the open state.[27,56,63,64]

4. Summary

In this review, we have summarized several studies in which fabricated large-area molecular electronic junctions fabricated by electrode-transfer method and characterized the electrical properties of the molecular junctions. The statistical analysis demonstrates the good reliability and reproducibility of these molecular junctions. To understand the charge transport mechanisms through the molecular junctions, theoretical models are employed. Simmons model explains nonresonant tunneling across the layers of benchmarking molecules such as fatty acid, alkanethiolates, and benzenethiolates. In particular, the unidirectional photoswitching is understood by the Landauer formalism which describes the transport by energetic parameters such as orbital energy and coupling strength. IETS or TVS are also utilized to investigate the vibrational modes or barrier height in the molecular junctions, respectively. In addition to the electrical characterization, various molecular junctions functionalized with diode, switch, and photoswitch characteristics are also demonstrated by the electrode-transfer method.

As introduced in this review, fabrication of the molecular electronic junctions by transferring the top gold or graphene electrode provides a reliable platform for studying the electronic transport properties of the molecular junctions. This platform has also the advantage of moderate junction yield obtained by avoiding direct metal deposition which is likely to generate the electrical shorted circuit.

1) A. Aviram and M. A. Ratner, Chem. Phys. Lett. **29**, 277 (1974).
2) B. Xu, X. Xiao, and N. J. Tao, J. Am. Chem. Soc. **125**, 16164 (2003).
3) F. Chen, J. Hihath, Z. Huang, X. Li, and N. J. Tao, Annu. Rev. Phys. Chem. **58**, 535 (2007).
4) D. J. Wold and D. C. Frisbie, J. Am. Chem. Soc. **123**, 5549 (2001).
5) H. Song, Y. Kim, H. Jeong, M. A. Reed, and T. Lee, J. Appl. Phys. **109**, 102419 (2011).
6) H. Song, Y. Kim, Y. Jang, H. Jeong, M. A. Reed, and T. Lee, Nature **462**, 1039 (2009).
7) J. Park et al., Nature **417**, 725 (2002).
8) M. Reed, C. Zhou, C. Muller, T. Burgin, and J. Tour, Science **278**, 252 (1997).
9) D. Xiang, H. Jeong, D. Kim, T. Lee, Y. Cheng, Q. Wang, and D. Mayer, Nano Lett. **13**, 2809 (2013).
10) C. J. Love, L. A. Estroff, J. K. Kriebel, R. G. Nuzzo, and G. M. Whitesides, Chem. Rev. **105**, 1103 (2005).
11) B. Mann and H. Kuhn, J. Appl. Phys. **42**, 4398 (1971).
12) E. Polymeropoulos and J. Sagiv, J. Chem. Phys. **69**, 1836 (1978).
13) A. V. Walker, T. B. Tighe, O. M. Cabarcos, M. D. Reinard, B. C. Haynie, S. Uppili, N. Winograd, and D. L. Allara, J. Am. Chem. Soc. **126**, 3954 (2004).
14) Z. Zhu, D. L. Allara, and N. Winograd, Appl. Surf. Sci. **252**, 6686 (2006).
15) H. Akkerman, D. M. de Leeuw, P. W. Blom, and B. de Boer, Nature **441**, 72 (2006).
16) D. Kim, H. Jeong, H. Lee, W.-T. Hwang, J. Wolf, E. Scheer, T. Huhn, H. Jeong, and T. Lee, Adv. Mater. **26**, 3968 (2014).
17) H. Jeong et al., Adv. Funct. Mater. **24**, 2472 (2014).
18) C. A. Nijhuis, W. F. Reus, J. R. Barber, M. D. Dickey, and G. M. Whitesides, Nano Lett. **10**, 3611 (2010).
19) L. Yuan, L. Jiang, D. Thompson, and C. A. Nijhuis, J. Am. Chem. Soc. **136**, 6554 (2014).
20) L. Jiang, S. C. Sangeeth, A. Wan, A. Vilan, and C. A. Nijhuis, J. Phys. Chem. C **119**, 960 (2014).
21) Y.-L. Loo, D. V. Lang, J. A. Rogers, and J. W. Hsu, Nano Lett. **3**, 917 (2003).
22) A. Vilan, A. Shanzer, and D. Cahen, Nature **404**, 166 (2000).
23) K. Shimizu, J. Fabbri, J. Jelincic, and N. Melosh, Adv. Mater. **18**, 1504 (2006).
24) H. Jeong et al., Nanotechnology **26**, 025601 (2015).
25) G. Wang, Y. Kim, M. Choe, T. Kim, and T. Lee, Adv. Mater. **23**, 755 (2011).
26) Y. Jang et al., Nanotechnology **27**, 145301 (2016).
27) J. Koo et al., ACS Appl. Mater. Inter **11**, 11645 (2019).
28) Y. Jang et al., ACS Appl. Mater. Inter **9**, 42043 (2017).
29) C. Zhou, M. Deshpande, M. Reed, L. Jones, and J. Tour, Appl. Phys. Lett. **71**, 611 (1997).
30) J. Chen, M. Reed, A. Rawlett, and J. Tour, Science **286**, 1550 (1999).
31) H. Haick and D. Cahen, Acc. Chem. Res. **41**, 359 (2008).
32) A. Vilan and D. Cahen, Adv. Funct. Mater. **12**, 807 (2002).
33) Y. Selzer and D. Cahen, Adv. Mater. **13**, 508 (2001).
34) A. Salomon, D. Berkovich, and D. Cahen, Appl. Phys. Lett. **82**, 1051 (2003).
35) P. C. Collier, J. O. Jeppesen, Y. Luo, J. Perkins, E. W. Wong, J. R. Heath, and F. J. Stoddart, J. Am. Chem. Soc. **123**, 12632 (2001).
36) H. Jeong et al., Appl. Phys. Lett. **106**, 063110 (2015).
37) N. Okabayashi, Y. Konda, and T. Komeda, Phys. Rev. Lett. **100**, 217801 (2008).
38) W. Wang, T. Lee, I. Kretzschmar, and M. A. Reed, Nano Lett. **4**, 643 (2004).
39) Y. Kim, T. Pietsch, A. Erbe, W. Belzig, and E. Scheer, Nano Lett. **11**, 3734 (2011).
40) B. Xu and N. J. Tao, Science **301**, 1221 (2003).
41) T.-W. Kim, G. Wang, H. Lee, and T. Lee, Nanotechnology **18**, 315204 (2007).
42) N. Tao, Nat. Nanotechnol. **1**, 181 (2006).
43) S. Choi, B. Kim, and D. C. Frisbie, Science **320**, 1482 (2008).
44) H. Akkerman and B. de Boer, J. Phys.: Condens. Matter **20**, 013001 (2008).
45) V. B. Engelkes, J. M. Beebe, and D. C. Frisbie, J. Am. Chem. Soc. **126**, 14287 (2004).
46) F. Chen, X. Li, J. Hihath, Z. Huang, and N. Tao, J. Am. Chem. Soc. **128**, 15874 (2006).
47) D. J. Wold, R. Haag, M. Rampi, and D. C. Frisbie, J. Phys. Chem. B **106**, 2813 (2002).
48) P. K. Hansma, Phys. Rep. **30**, 145 (1977).
49) C. Adkins and W. Phillips, J. Phys. C: Solid State Phys. **18**, 1313 (2000).
50) L.-L. Lin, C.-K. Wang, and Y. Luo, ACS Nano **5**, 2257 (2011).
51) T. Han, T. Kwon, N. Li, H. Seo, W. Xu, K. S. Kim, and T. Lee, Angew. Chem. Int. Ed. **55**, 6197 (2016).
52) J. M. Beebe, B. Kim, D. C. Frisbie, and J. G. Kushmerick, ACS Nano **2**, 827 (2008).
53) J. M. Beebe, B. Kim, J. Gadzuk, D. C. Frisbie, and J. G. Kushmerick, Phys. Rev. Lett. **97**, 026801 (2006).
54) M. Irie, S. Kobatake, and M. Horichi, Science **291**, 1769 (2001).
55) A. C. Whalley, M. L. Steigerwald, X. Guo, and C. Nuckolls, J. Am. Chem. Soc. **129**, 12590 (2007).
56) D. Dulić, S. van der Molen, T. Kudernac, H. Jonkman, J. de Jong, T. Bowden, J. van Esch, B. Feringa, and B. van Wees, Phys. Rev. Lett. **91**, 207402 (2003).
57) M. Zhuang and M. Ernzerhof, J. Chem. Phys. **130**, 114704 (2009).
58) A. J. Kronemeijer, H. B. Akkerman, T. Kudernac, B. J. van Wees, B. L. Feringa, P. W. Blom, and B. de Boer, Adv. Mater. **20**, 1467 (2008).
59) T. Sendler et al., Adv. Sci. **2**, 1500017 (2015).
60) S. van der Molen, J. Liao, T. Kudernac, J. S. Agustsson, L. Bernard, M. Calame, B. J. van Wees, B. L. Feringa, and C. Schönenberger, Nano Lett. **9**, 76 (2009).
61) C. Jia et al., Science **352**, 1443 (2016).
62) C. Jia, J. Wang, C. Yao, Y. Cao, Y. Zhong, Z. Liu, Z. Liu, and X. Guo, Angew. Chem. Int. Ed. **52**, 8666 (2013).
63) M. J. Comstock et al., Phys. Rev. Lett. **99**, 038301 (2006).
64) C. Gahl, R. Schmidt, D. Brete, E. R. McNellis, W. Freyer, R. Carley, K. Reuter, and M. Weinelt, J. Am. Chem. Soc. **132**, 1831 (2010).